IEEE Access
Multidisciplinary | Rapid Review | Open Access Journal

Received 30 September 2022, accepted 15 November 2022, date of publication 21 November 2022,
date of current version 30 November 2022.

Digital Object Identifier 10.1109/ACCESS.2022.3223707

APPLIED RESEARCH

Detection and Quantification of Root-Knot Nematode (Meloidogyne Spp.) Eggs in Tomato Plants Using Image Analysis

TOP BAHADUR PUN[1], ARJUN NEUPANE[2], RICHARD KOECH[3], AND KIRSTY J. OWEN[4]

[1]School of Engineering and Technology, Central Queensland University, Bundaberg, QLD 4760, Australia
[2]School of Engineering and Technology, Central Queensland University, Rockhampton, QLD 4700, Australia
[3]School of Health, Medical and Applied Sciences, Central Queensland University, Bundaberg, QLD 4760, Australia
[4]Centre for Crop Health, Institute for Life Sciences and the Environment, University of Southern Queensland, Toowoomba, QLD 4305, Australia

Corresponding author: Top Bahadur Pun (topbahadur.pun@cqumail.com)

This work was supported by the Research Training Program (RTP) Scholarship Funded by the Australian Government and Resources Provided by Central Queensland University, Australia.

ABSTRACT Root-knot nematodes (*Meloidogyne* spp.; RKN) are major plant-parasitic nematodes that cause significant loss to agricultural production. An accurate assessment of the RKN population density at a field level is crucial for decisions about the application of control measures to minimise yield losses. Traditionally, RKN populations are identified and counted by nematologists using a microscope. This method is a specialised, time-consuming process and prone to errors. In our study, we investigated three semi-automated methods to detect and count RKN eggs using image analysis: contour arc (CA), skeleton structure (SS), and extreme point (EP). These methods were used to automate the length measurement of RKN eggs, and the results were compared with traditional methods of quantification. The EP method produced the highest correlation with the manual length measurement of RKN eggs. Further, these methods were used to detect and count RKN eggs to quantify low and highly cluttered images. We estimated the optimal range of the ratio of each method to detect and count RKN eggs. Overall, the EP method computed using mid-width of RKN eggs revealed better detection and counting of RKN eggs as compared to the SS and CA methods. A counting correlation up to $R^2 = 0.905$ was obtained. This study found that the difference between mid-width and the average width of RKN eggs and soil particles could be used to discriminate 70-80 % of soil particles. Our research thus contributes a new feature that can be used to discriminate or classify objects in object detection techniques.

INDEX TERMS Plant-parasitic nematode, root-knot nematode egg, computer-vision, image analysis, nematode egg detection, image segmentation, morphological-analysis, medial-axis transform, root-knot nematode detection.

I. INTRODUCTION

Nematodes are ecologically diverse microfauna and bioindicators adaptive to different habitats, providing evolutionary benefits for their survival [1], [2]. The continuous evolution of nematodes in the rhizosphere and the dynamic relation between nematodes and plants resulted in plant-parasitic nematodes [3], [4]. Plant-parasitic nematodes (PPN) are attracted to the roots of host plants through semiochemicals produced by roots [5], [6], [7]. PPN damage the root tissues of plants. Some nematodes remain outside of plant roots (ectoparasites), whereas others enter roots to complete their life cycle (endoparasites) [4]. Nematode-induced distress does not directly originate from cell death or necrosis but is caused by the interference in the root system which obstructs plants from absorbing nutrients from the rhizosphere [8]. Among these endoparasitic nematodes, root-knot nematodes (*Meloidogyne* spp.; RKN), cyst nematodes

The associate editor coordinating the review of this manuscript and approving it for publication was Tao Zhou.

(including *Heterodera* spp. and *Globodera* spp.), and root lesion nematodes (*Pratylenchus* spp.) are the top three PPN with economic importance [9].

Plant-parasitic nematodes (PPN) can be major limiting factors to crop and vegetable production worldwide. In the US, PPN damage to crops is estimated to be US $80-110 billion per year [10], [11]. It is estimated that PPN cause 5-20% losses in crop yield worth over AU$80 million in Australia [12], [13].

On average, RKN cause 10-20 % yield loss in horticultural crops [14]. Australian growers lost around AU$123 million in one year due to root-lesion nematodes [15]. These nematodes need to be identified and quantified so that farmers can be advised on the appropriate nematode treatment options [16]. Thus, an appropriate quantification method is required to assess plant-parasitic nematodes before applying control measures. Various methods have been developed to identify nematodes including morphology, molecular and differential host test [17]. RKN infestation can be determined based on the number of eggs in the roots [18], [19], juvenile populations in the soil [20], [21], the number of adult females in the roots [22], [23], and root gall index and reproduction factor [24]. The number of egg mass and gall rating are also used for nematode infestation [25].

Females of RKN and cyst nematode remain inside plant roots to complete their lifecycle. The duration of the nematode's life cycle is influenced by environmental factors such as temperature, host plant, and species [26]. The juveniles in the second stage move through root tissues until a suitable feeding site is found. Once the feeding site is established, they moult several times to become adults. After three weeks of growth, the female RKN lays eggs in the gelatinous matrix [8], which protects the eggs against predators or microorganisms [27], [28]. These nematode species can lay 50 to 500 eggs per female. RKN egg size and shapes vary, and the average egg is 95 μm in length and 40 μm wide [26]. The length of the second stage juveniles of different species of RKN ranges from 250 to 600 μm. Depending on environmental factors, some second-stage juveniles remain in the egg state through winter [28], [29]. Plant-parasitic nematodes mature from first (J1) to second stage larvae (J2) inside the egg. *Heterodera glycines* can take 172 hours to develop from a single-celled egg to a fully grown second-stage juvenile [30]. Thus, the assessment of plant-parasitic nematodes includes quantifying eggs for complete and precise quantification of plant-parasitic nematode population [31], [32], [33].

Nematodes are not only parasitic to plants but also to animals. Some studies focused on identifying and counting animal parasitic nematodes eggs in faecal matter to estimate the burden on the gastrointestinal tract of animals [34] have been undertaken. Worm egg count is essential for knowing when to implement controls to prevent disease and improve livestock growth. Roberts and Swan [35] found a strong correlation (r=0.83) between the number of eggs and the number of *Haemonchus contortus* vermiform stages, suggesting that it is beneficial to predict the level of infection. Ostergaard [36] investigated image processing techniques to detect and characterise eggs of intestinal parasites. The image processing techniques such as thresholding, filtering, morphological operation, colour plane extraction, and image calibration for measurement were explored to detect parasite eggs [36]. The study found that image processing methods were statistically significant in differentiating parasite eggs and suggested the use of automated image processing methods for parasite egg detection and identification.

Similarly, Huang et al. [21] developed a method to count gastrointestinal eggs of parasites. Faecal egg counting requires sample processing to separate eggs from faeces. Stained eggs in a McMaster chamber were captured using a fluorescence microscope or smartphone. The images were processed using ImageJ software to count particles with a specific range of pixels.

Few studies have used machine learning techniques to detect and count plant parasitic nematodes. A deep learning model was used to count soyabean cyst nematodes (SCN) eggs in a high cluttered image without significant changes in accuracy. Moreover, Qazi et al. [37] proposed real-time identification of nematode eggs in terms of genus and species. The investigation showed that photoluminescence spectral measurement could discriminate species of nematode eggs as each species of nematodes has a distinct emission spectrum. These studies used different sensors to discern plant-parasitic nematodes from soil and plants and animal parasitic nematode eggs from faeces. However, to the best of our knowledge, RKN eggs have not been detected using image analysis. Most nematode infestation assessments in literature used both the number of juveniles and the number of eggs in the roots [38], [39]. RKN juveniles were quantified for the assessment of RKN populations using image analysis [40]. Thus, this study aimed to investigate RKN egg size and detect RKN eggs in terms of their length, width, and the ratio of length to width. This study used a new feature to discriminate between RKN eggs and soil particles based on the difference between the mid-width and average width of RKN eggs. In addition, a novel extreme point (EP) method was used to analyse the size and detect eggs. This study also determined the optimal ratio range to detect and count RKN eggs. Further, the morphological features (length, mid-width, average-width, and the difference between mid-width and average width measurement) were analysed to detect and count RKN eggs.

II. METHODS

The detection of RKN eggs was carried out using the detection model depicted in Fig. 1. Initially, a sample of RKN eggs was prepared and collected. The samples were processed using the Hussey and Barker method [41]. Then, images of RKN eggs were captured and analysed using image processing techniques. Finally, eggs in the images were measured, counted, and compared with manual

quantification. These procedures are described in detail in the following sections.

A. SOIL SAMPLE PREPARATION AND EGG COLLECTION

Tomato plants were grown in propagating sand and potting mix in a greenhouse located at 24°54′5″ S, 152°18′45″ E, Central Queensland University (CQU), Bundaberg Campus, Queensland, Australia. The greenhouse temperature was maintained at 20 ±5 °C with 12 hours light/12 hours dark. The tomato plants were inoculated with RKN eggs (Meloidogyne incognita) after 1 to 1.5 months of plant growth. Then, the plants were grown with regular irrigation for a further 1 to 1.5 months. Subsequently, a few plants were pulled out of the container to check for the presence of root galls to confirm infestation by RKN. If galls were present, plants were then removed from the pots, the plant tops removed, and the roots collected and gently washed free of the sand: soil mix. These root samples were processed at the CQU's Science laboratory located in the Bundaberg Campus using the Hussey and Barker method [41]. This involved cutting the tomato plant roots into less than 1 cm pieces and stirring them gently with a glass rod in a 0.5% sodium hypochlorite (NaClO) solution for 5 minutes. Subsequently, the root pieces were washed on a 25 μm-aperture sieve stacked on 150 μ-aperture sieve. The residue was collected in 450 ml water from a 25 μm-aperture sieve using a wash bottle. After collection of the eggs from the root tissue, a 5 ml egg sample was put in the petri dish and placed on the microscope stage.

B. IMAGE ACQUISITION

Initially, images of RKN eggs were captured using Olympus DP73 camera attached to the Olympus BX53 microscope. The images were captured on high contrast, ISO 200 sensitivity settings and saved in a 1600 × 1200 size frame. The 4x objective lens was selected for this study. With these settings, RKN eggs were viewed on the microscope while adjusting the focus to take clear images. CellSens software was installed in the computer and utilised to acquire images and measure dimensions manually. Once all the camera parameters were set, images of RKN were taken at the proper focus and saved in a jpg format. Then, the copies of the images were measured manually. The measurements of 111 RKN eggs are described in the 'manual and automated measurement' section.

C. IMAGE ANALYSIS AND PROCESSING

The captured RGB (red, green, and blue) images were converted to gray images for RKN eggs detection. A segmentation technique was applied to distinguish soil particles from RKN eggs in the images. The triangle threshold method was implemented to segment gray images (Fig. 2(a)) into binary image (Fig. 2(b)) [42]. Among other thresholding methods, the triangle threshold method was found to be the best in segmenting rice roots [43]. We investigated other thresholding methods such as Otsu, MaxEntropy, Yen method and found the triangle method to be the most suitable for segmenting RKN egg images. The triangle threshold of pixel value (T) was computed as the longest distance between the histogram and the line from histogram peak to base point [42]. To compute the threshold value (T), we first computed the line between the highest and the lowest grayscale value in the histogram of gray images. The distance between the histogram and each point on the line was calculated. Finally, we selected pixel intensity value as threshold (T) that has maximum distance between histogram and the line. The threshold of image g(x, y) is defined as shown in Equation 1.

$$g(x, y) = \begin{cases} 1, & if\ f\ (x, y) > T \\ 0, & if\ f\ (x, y) < T \end{cases} \quad (1)$$

where T is the threshold value at point (x, y)

$f\ (x, y)$ is the gray level of the image pixel.

Subsequently, the soil particles smaller than the minimum RKN egg size were removed using a morphological operation (Fig. 3(a)). To do this, we determined the size of the connected component of the pixel. If the component size was less than the smallest size of the RKN egg, then we removed the connected components. The connected components larger than the minimum egg size remained in the image. Furthermore, a morphological closing operation was applied to restore the missing edges of the foreground object (Fig. 3(b)). The closing operation involved dilation of the object followed by an erosion operation. This operation joined the broken section and narrowed down the gap in the contour [44]. The morphological opening operation was employed in the skeleton method to avoid unnecessary branch formation in the skeleton. The morphological opening operation comes in handy to smooth contours and remove sharp peaks or caps [45]. The holes inside the object were filled. Ultimately, each contour in the image was detected to compute the size of the object. For size analysis, the length of RKN eggs was computed using contour arc (CA), skeleton structure (SS), and extreme point (EP) methods. These methods are described in the 'egg measurement and quantification' section. The width of RKN eggs was measured at the middle of the egg. The measured values were saved in a Microsoft excel file. Then, we computed descriptive statistics such as minimum and maximum values of the ratio. Similarly, we calculated minimum and maximum area from 111 RKN eggs using OpenCV function based on Green Theorem [46] as shown in Algorithm 1. The minimum and maximum value of ratio and area were used in Algorithm 2. These values were implemented in the algorithm to detect and count RKN eggs. The algorithm computed egg sizes based on CA, SS, and EP methods as shown in Algorithm 2. The automated measurement was compared with manual measurement. The correlation between manual measurement and machine measurement was observed using the coefficient of determination (R^2) and mean absolute error (MAE) metrics.

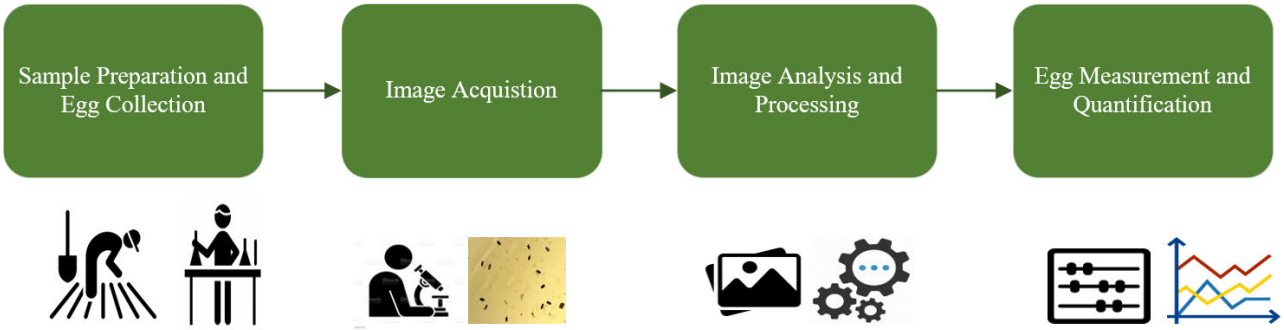

FIGURE 1. Nematode egg detection and counting framework.

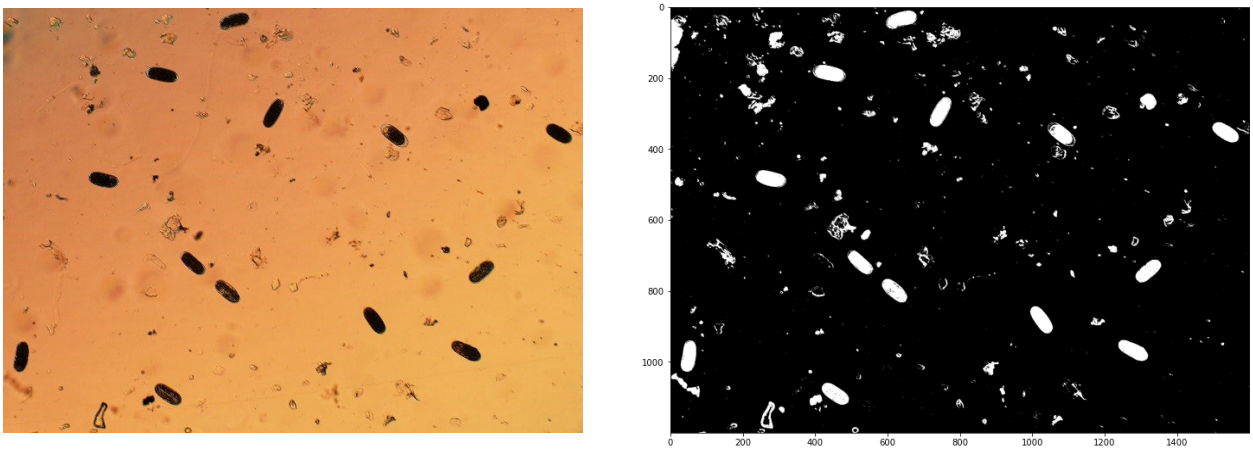

FIGURE 2. (a) Sample image of root-knot nematode (RKN) eggs; (b) Triangle threshold segmentation of root-knot nematode (RKN) egg image.

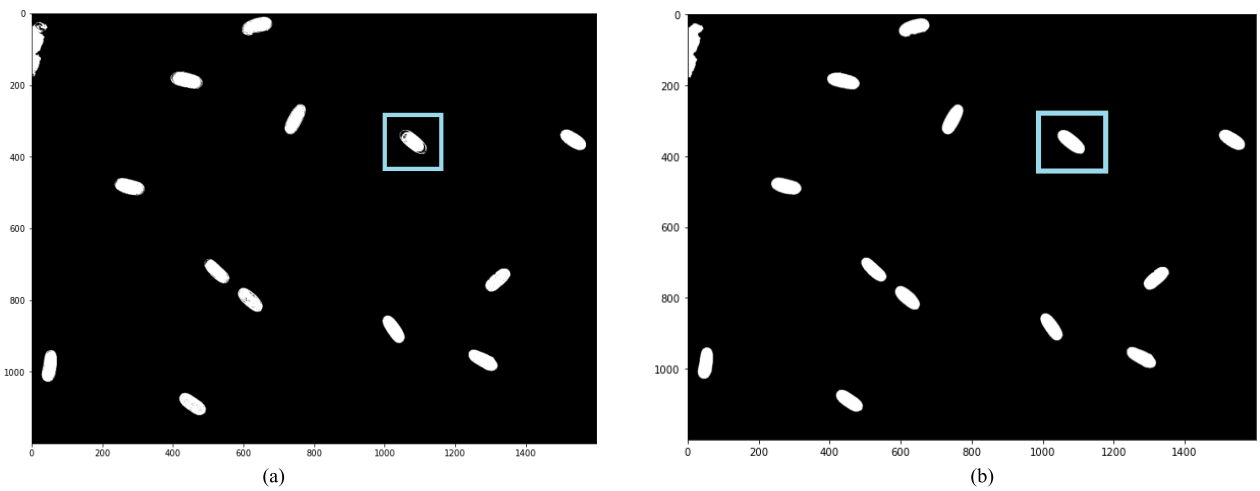

FIGURE 3. (a) Binary image after small particles were removed using morphological operation; (b) morphological closing and filling operation of root-knot nematode (RKN) egg in rectangular box.

D. EGG MEASUREMENT AND QUANTIFICATION OF RKN

1) EGG LENGTH COMPUTATION

The length of RKN eggs was computed using contour perimeter length, skeleton structure, and extreme point distance. The contour of an RKN egg in Fig. 4(a) was computed using computer vision, as shown in Fig. 4(b). The perimeter of the contour was divided into one half to obtain the length of the eggs. Then, half of the contour

Algorithm 1 Compute Area of Contour Using Green Theorem

Input: contour points: (x_0, y_0),(x_1, y_1),(x_2, y_2),.(x_{n-1}, y_{n-1}), (x_n, y_n) where n is number of points, (x_k, y_k) is k^{th} point ordered in counter clockwise direction.
Output: Area of contour
Compute $area(a)=\sum_{n=0}^{k} 1/2(x_{k+1}+x_k)(y_{k+1}-y_k)$
Return $area\ (a)$

Algorithm 2 Pseudocode for Root-Knot Nematode Egg Detection

1. Load image (Img (x, y))
2. Convert RGB image to gray, f (x, y) =Gray (Img (x, y))
3. Apply triangle thresholding (T) to gray image

$$Img(x,y) = \begin{cases} 1, & if\ f\ (x,y) > T \\ 0, & if\ f\ (x,y) < T \end{cases}$$

a) Apply morphological small particle removal operation
b) Apply morphological closing operation
c) Fill holes in the image
d) Find all contours(c) in the image (Img (x, y))
e) **For** each contour(c):
if (Minimum Area<contourArea(c)<Maximum Area)
a. Create mask of each contour
b. Compute Width, Length, Ratio and Area
c. **if** (Minimum Ratio < ratio < Maximum Ratio):
- contourArea(c)= RKN
- Save mask image and measurement

d. **else**
- contourArea(c)=Soil Particle or Rubbish

e. Save Image

perimeter was computed as the length of RKN. In the second method, eggs were then converted to skeleton structure using morphological thinning operation (Fig. 4 (c)). The largest length of the skeleton branch was computed as the length of RKN eggs [47]. In the third method, extreme pixels of RKN eggs were identified as the farthest endpoints from the centre in the four directions, as shown in Fig. 4(d). The largest Euclidian distance between any two extreme points was estimated as the length of RKN eggs.

2) RKN EGG WIDTH COMPUTATION

The width of RKN eggs was computed at the middle part of egg to identify and discriminate between eggs and soil particles. The mid-point of the egg was computed using the centroid of the blob known as the image moment. The width at mid-point was estimated using the distance transform of the medial axis. The distance transform of the medial axis is the distance to the boundary from all medial axis points [48]. The width at the middle of RKN egg and the average width of RKN egg was used to estimate the size of the RKN eggs. The difference between the mid-width and average width was used to discriminate eggs from soil particles.

3) RKN EGG RATIO COMPUTATION

To compute the ratio, first, we calculated the difference between RKN egg length and mid-width / average-width and then the ratio was computed as the difference to the mid-width, as shown in Table 1. The ratio of length to mid-width could not distinguish RKN eggs from soil particles. Thus, the difference between the length and mid-width/average-width was calculated to discriminate between elliptical structures and other shapes. The length of the egg represented the major-axis of ellipse, whereas the width denoted the minor-axis of the ellipse (Fig 5). The vertical and the horizonal lines in Fig. 5 indicate the length and mid-width of RKN egg (major-axis and minor-axis of ellipse), respectively. Thus, we used the difference between the length and mid-width in the ratio to capture the elliptical structure of RKN eggs.

TABLE 1. Ratio specifications of root-knot nematode (rkn) eggs.

Width	Method	Ratio
Mid-width	Contour Arc	(Length−Mid-width)/ Mid-width
	Skeleton Structure	Length/Mid-width
	Extreme Point	(Length−Mid-width)/Mid-width
Average-width	Contour Arc	(Length−Average-width)/ Average-width
	Skeleton Structure	Length/ Average-width
	Extreme Point	(Length−Average-width)/ Average-width

III. EVALUATION CRITERIA

A. MANUAL AND AUTOMATED MEASUREMENT

The length and width of RKN eggs were measured manually using cellSens software. The length was measured as the maximum longitudinal distance of the RKN egg in the image. The mid-width of RKN eggs was measured at the centre of the RKN eggs. The average-width of RKN eggs was measured at three equal intervals on the body of RKN eggs (Fig. 6(a) and (b)). The distribution of manually measured length, width, and ratio are shown in Fig. 8 using a density plot. The automated measurement of the length was computed using three approaches: contour arc (CA), skeleton structure (SS), and Extreme point (EP). The width of the egg was measured based on the average width and the mid-width. The ratio was computed as shown in Table 1 The manual and automated measurements were assessed using Coefficient of Determination (R^2), and Mean Absolute Error (MAE), Mean Absolute Percentage Error (MAPE).

B. CO-EFFICIENT OF DETERMINATION (R^2)

The coefficient of determination was used to characterise the proportion of variance explained by the statistical model [49]. R^2 computes the percentage of the variance of the response variable resolved by a linear relationship with explanatory variables. It is defined as the ratio of explained and the total sum of squares [50]:

$$R^2 = ESS/TSS = 1 - RSS/TSS$$

where RSS, ESS, and TSS are residual, explained, and the total sum of squares, respectively.

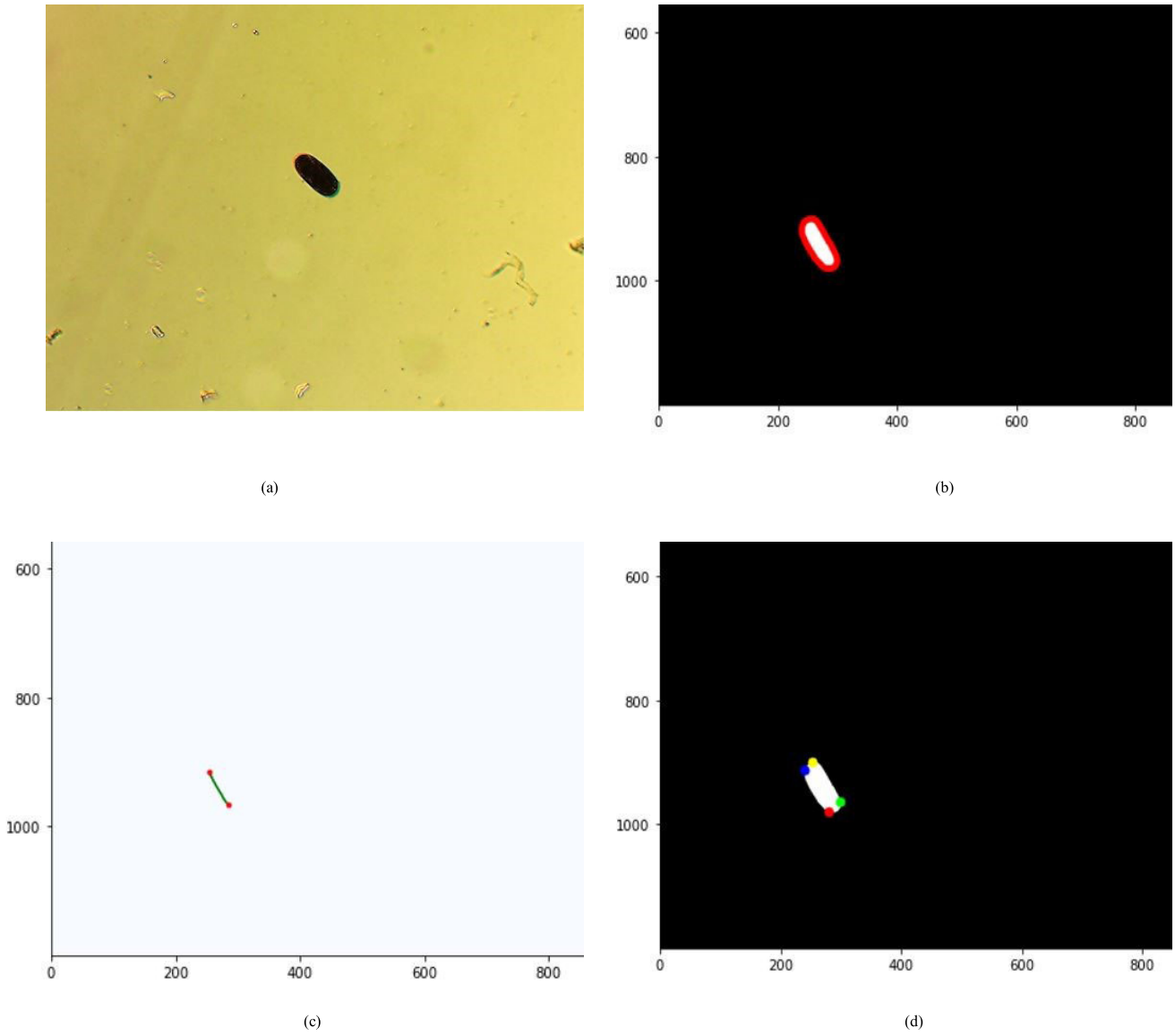

FIGURE 4. (a) Colour image of root-knot nematode (RKN) egg; (b) Root-knot nematode (RKN) egg with contour structure; (c) Skeleton structure of root-knot nematode (RKN) egg;(d) Root-knot nematode (RKN) egg with extreme point.

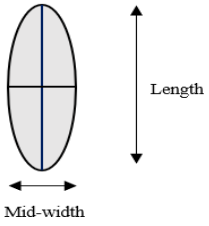

FIGURE 5. Schematic diagram of root-knot nematode (RKN) egg.

C. MEAN ABSOLUTE ERROR (MAE)

Mean absolute error is defined as the sum of the absolute difference between actual value (y) and predicted value (y') [51]. MAE is most suitable for natural measures of average error magnitude. It is suitable for the evaluation of any dimension and comparison of model performance [52].

$$MAE = 1/n \sum_{1}^{n} |y - y'|$$

where y is actual value, and y' is predicted value and n is number of samples.

D. MEAN ABSOLUTE PERCENTAGE ERROR (MAPE)

Mean absolute percentage error is one of the most popular error metrics used in prediction or detection methods because of its scale consistency [53]. It provides an easily comprehensible gauge of error [54]. Mathematically, MAPE is defined as [55]:

$$\text{MAPE} = 1/n \sum_{1}^{n} \frac{|\text{y} - \text{y}'|}{y}$$

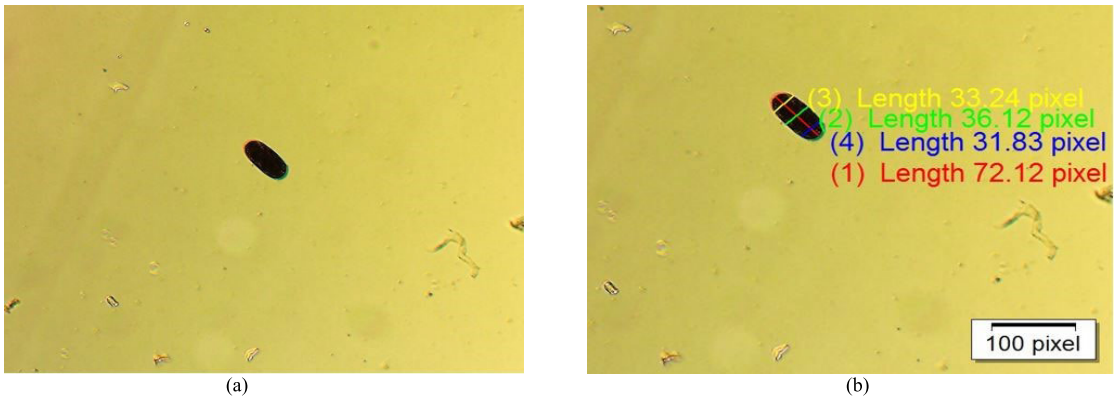

FIGURE 6. (a) Sample image of root-knot nematode (RKN) egg; (b) manual measurement of root-knot nematode (RKN) egg.

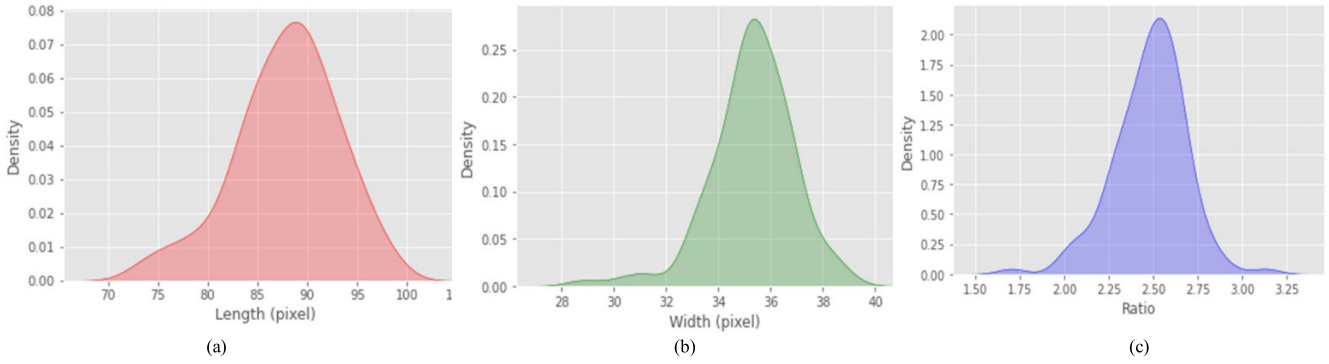

FIGURE 7. Distribution of manual measurement of Root-knot nematodes (RKN) eggs (a) length distribution of root-knot nematode (RKN) eggs, (b) width distribution of root-knot nematode eggs, (c) ratio distribution of root-knot nematode eggs.

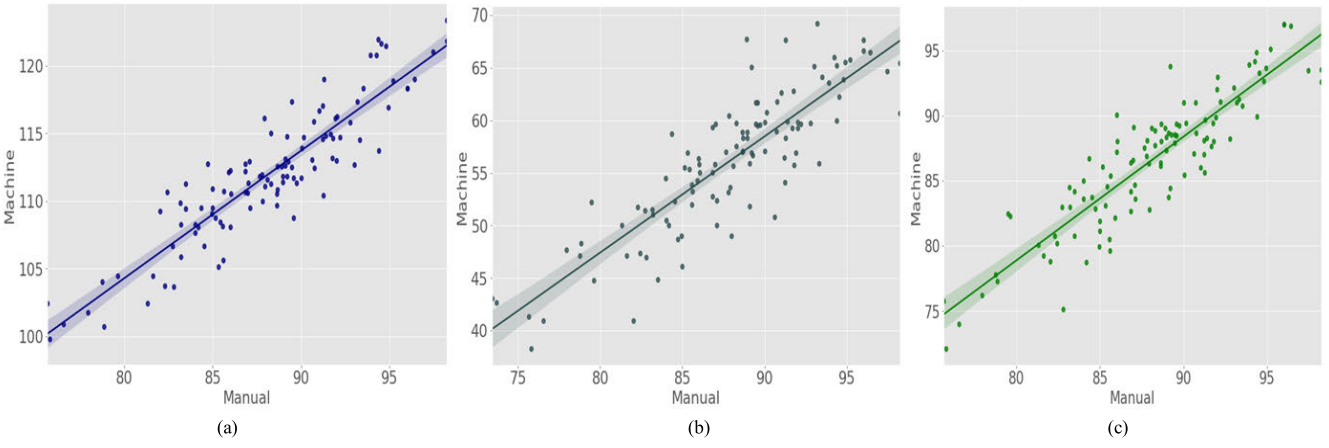

FIGURE 8. Automated and manual measurement of root-knot nematode eggs length using mid- width (a) contour arc (b) skeleton structure, and (c) extreme point methods.

where y is actual value, and y' is predicted value and n is number of samples.

IV. RESULT AND DISCUSSION

Traditionally, RKN eggs are quantified by observing a sample on a microscope and manually counted by a nematologist. Although identifying and counting RKN eggs is relatively simple based on this traditional method, it requires considerable time both in training to identify nematodes morphologically and assess a sample, can cause eye strain, and is prone to errors as the number of samples and density increases. This study presented alternative automated methods of detecting and counting RKN eggs. To discern and count the RKN eggs, the manual measurements of RKN

TABLE 2. Comparison between automated and manual length of root-knot nematode (rkn) eggs using mid-width and average-width.

Width Computation method	Length Computation method	Coefficient of Determination (R^2)	Mean Absolute Error (MAE)	Mean Absolute Percentage Error (MAPE)
Mid-width	Contour Arc	0.827	23.834	0.271
	Skeleton Structure	0.737	31.740	0.362
	Extreme Point	0.804	2.148	0.024
Average-Width	Contour Arc	0.804	24.457	0.278
	Skeleton Structure	0.602	29.539	0.337
	Extreme Point	0.802	2.159	0.024

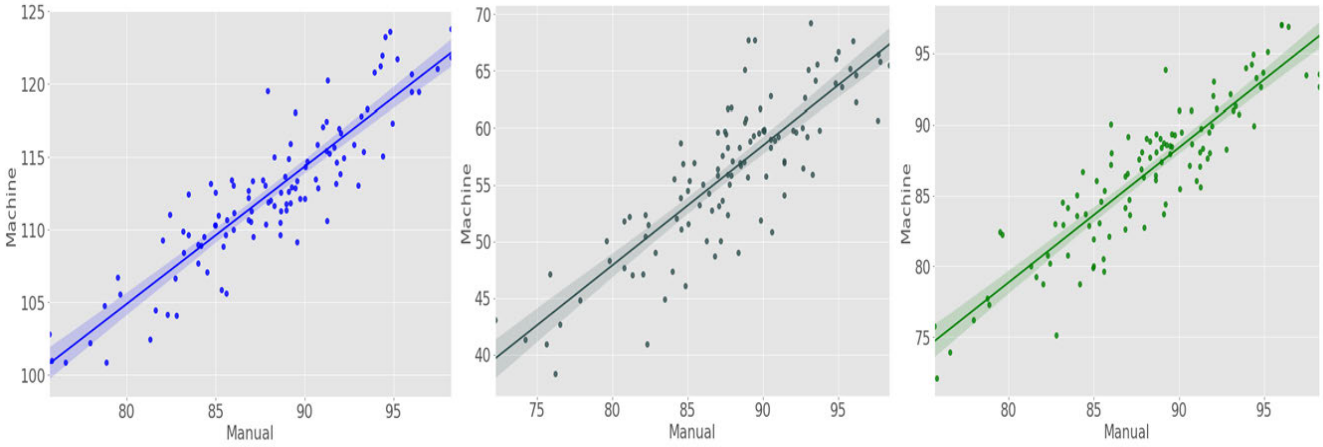

FIGURE 9. Automated and manual measurement of root-knot nematode (RKN) egg length using average- width (a) contour arc (b) skeleton structure, and (c) extreme point methods.

TABLE 3. Comparison of ratio based on different length measurement methods.

Ratio Specification	Length Computation method	Coefficient of Determination (R^2)	Mean Absolute Error (MAE)	Mean Absolute Percentage Error (MAPE)
(Length – Mid-Width)/Mid-width	Contour Arc	0.424	0.342	0.120
Length/Mid-width	Skeleton Structure	0.540	0.930	0.375
(Length – Mid-Width)/Mid-width	Extreme Point	0.522	0.125	0.083
(Length – Average-width)/ Average-width	Contour Arc	0.022	1.063	0.620
Length/ Average-width	Skeleton Structure	0.257	0.213	0.118
(Length – Average-width)/Average-width	Extreme Point	0.075	0.522	0.210

eggs were compared with automated measurements. The distribution of the manual measurements is shown in Fig. 7. The automated measurements were computed using the CA, SS, and EP methods. These measurements were evaluated in terms of coefficient of determination (R^2), mean absolute error (MAE), and mean absolute percentage error (MAPE). One hundred and eleven RKN eggs were measured manually and using an automated method. Further, the images were classified based on two categories: low cluttered and high cluttered. There were 733 low cluttered images having a total of 1908 RKN eggs and 203 high cluttered images consisting of 1526 RKN eggs.

This study used the RGB image analysis method to detect and count RKN eggs. The CA and SS methods were initially applied to detect RKN juveniles but can also be used to detect and count RKN eggs. In addition, the new approach of

TABLE 4. Comparison of automated and manual root-knot nematode (rkn) egg count with ratio variation (low-cluttered).

Ratio Range based on mid-width	Method	Coefficient of Determination (R^2)	Mean Absolute Error (MAE)	Mean Absolute Percentage Error (MAPE)	Misidentified Root-knot nematode eggs	Egg Detected	Undetected Root-knot nematode eggs
	Contour Arc	0.356	0.984	0.382	9	1195	713
0.6-2.2	Skeleton Structure	0.739	0.237	0.094	79	1813	95
	Extreme Point	0.873	0.120	0.041	62	1882	26
	Contour Arc	0.356	0.984	0.382	9	1195	713
0.7-2.2	Skeleton Structure	0.746	0.231	0.092	74	1812	96
	Extreme Point	0.884	0.105	0.035	50	1881	27
	Contour Arc	0.356	0.984	0.382	9	1195	713
0.8-2.2	Skeleton Structure	0.746	0.233	0.094	72	1809	99
	Extreme Point	**0.905**	**0.088**	**0.028**	**35**	**1878**	**30**
	Contour Arc	0.693	0.306	0.120	27	1710	198
0.7-2.5	Skeleton Structure	**0.788**	**0.192**	**0.074**	**93**	**1860**	**48**
	Extreme Point	0.889	0.100	0.035	55	1889	19
	Contour Arc	0.868	0.117	0.042	51	1873	35
0.7-3	Skeleton Structure	0.784	0.210	0.080	124	1878	30
	Extreme Point	0.873	0.122	0.044	73	1891	17
	Contour Arc	**0.883**	**0.103**	**0.037**	**60**	**1892**	**16**
0.7-3.5	Skeleton Structure	0.761	0.238	0.092	149	1882	26
	Extreme Point	0.839	0.151	0.055	94	1891	17
	Contour Arc	0.878	0.115	0.042	72	1895	13
0.7-4	Skeleton Structure	0.722	0.271	0.104	175	1884	24
	Extreme Point	0.825	0.171	0.062	110	1892	16

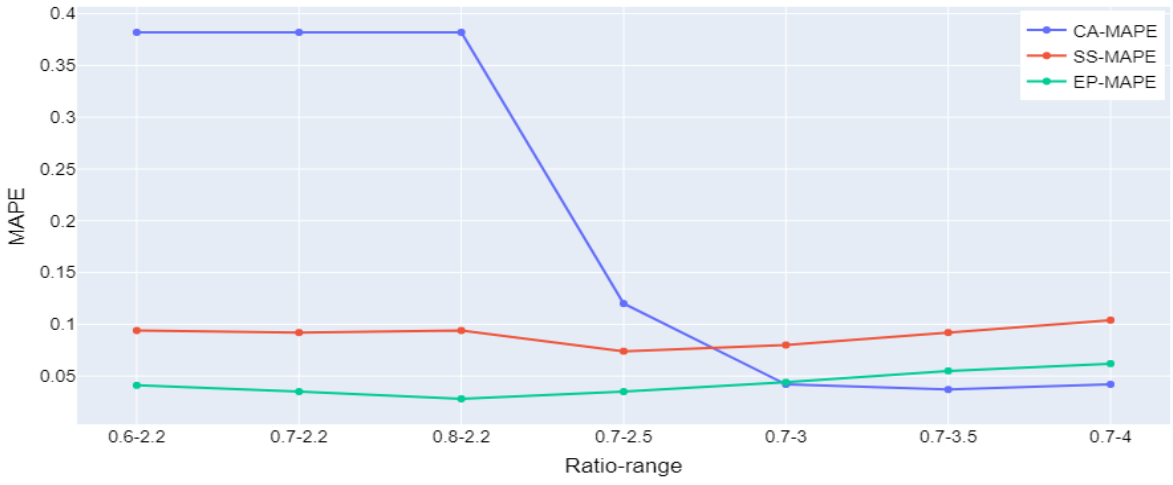

FIGURE 10. Line plot of MAPE based on contour arc (CA), skeleton structure (SS) and extreme point (EP) methods.

extreme point (EP) was used to detect and count RKN eggs. The length of RKN eggs was computed using the CA, SS, and EP. The comparison of manual and automated measurements of length based on contour arc (CA), skeleton structure (SS), and the extreme point (EP) is shown in Fig. 8.

The length of RKN eggs was computed using EP based on mid-width and found the highest accuracy with $R^2 = 0.827$, MAE=23.834, and MAPE=0.271 (Table 2). Also, the automated computed length variance was less than the CA and SS. Further, these methods were investigated using average-width. The graphical representation of manual and automated measurement using average width is shown in Fig. 9. The correlation of length of RKN eggs was slightly less than using mid-width.

The ratio of RKN eggs (as shown in Table 1) computed by proposed method was highly correlated with manual measurement using mid-width than the average-width.

The ratio of RKN eggs was highly correlated with the manual measurement compared to RKN juvenile [40]. The skeleton structure had the highest correlation between

TABLE 5. Comparison of automated and manual root-knot nematode (rkn) eggs count with ratio variation (high-cluttered).

Ratio Range based on mid-width	Method	Coefficient of Determination (R^2)	Mean Absolute Error (MAE)	Mean Absolute Percentage Error (MAPE)	Misidentified Root-knot nematode eggs	Detected Root-knot nematode eggs	Undetected Root-knot nematode eggs
	Contour Arc	0.662	1.133	0.145	10	1306	220
0.6-2.2	Skeleton Structure	0.801	0.586	0.080	60	1467	59
	Extreme Point	0.881	0.438	0.061	66	1503	23
	Contour Arc	0.662	1.133	0.145	10	1306	220
0.7-2.2	Skeleton Structure	0.809	0.571	0.077	55	1465	61
	Extreme Point	**0.888**	**0.433**	**0.060**	**57**	**1495**	**31**
	Contour Arc	0.662	1.133	0.145	10	1306	220
0.8-2.2	Skeleton Structure	**0.807**	**0.586**	**0.079**	**49**	**1456**	**70**
	Extreme Point	0.835	0.522	0.072	51	1471	55
	Contour Arc	0.803	0.581	0.075	36	1444	82
0.7-2.5	Skeleton Structure	0.790	0.600	0.083	87	1491	35
	Extreme Point	0.873	0.482	0.068	71	1499	27
	Contour Arc	**0.844**	**0.487**	**0.064**	**56**	**1483**	**43**
0.7-3	Skeleton Structure	0.782	0.689	0.097	118	1504	22
	Extreme Point	0.859	0.536	0.076	86	1503	23
	Contour Arc	0.834	0.532	0.072	75	1493	33
0.7-3.5	Skeleton Structure	0.772	0.802	0.112	144	1507	19
	Extreme Point	0.853	0.566	0.082	96	1507	19
	Contour Arc	0.827	0.551	0.076	86	1500	26
0.7-4	Skeleton Structure	0.755	0.901	0.126	167	1510	16
	Extreme Point	0.834	0.615	0.088	108	1509	17

the manual and automated ratio computation with R^2 of 0.540 (Table 3). The reason behind the high correlation of ratio was because of the clear representation of RKN egg using skeleton structure. The width of the RKN eggs were computed using distance transform in the middle part of RKN eggs and the average width of RKN eggs. The difference between the mid-width and average width of the RKN egg was computed as a discriminable feature of RKN eggs. The difference between the average width and mid-width of RKN eggs and soil particles was analysed to find the differences between RKN eggs and soil particles. The result showed that 70-80% of soil particles misidentified as RKN eggs had a width greater than 20 pixels. This approach was accurate for all the methods except the EP method used with mid-width of the egg. The EP method effectively discriminated the RKN eggs and soil particles based on the elliptical shape analysis. The width difference was low for the bean-shaped egg whereas it was high with objects that were more circular in shape.

Further, the CA, SS, and EP methods were employed to detect and count RKN eggs in the low- and high- cluttered images based on mid-width. Then, the comparison between manual eggs count was compared with automated eggs count (Table 4 and Table 5, respectively). The CA, SS, and EP methods were used to compute optimal detection of RKN eggs at a different ratio range. The detection at the optimal range discerns a maximum number of RKN eggs and reduces unnecessary image processing and analysis burden of soil particles or root tissue. The EP method had the highest correlation between manual and automated egg count at a ratio range 0.8 - 2.2 in low cluttered images with $R^2 = 0.905$, MAE = 0.088, and MAPE = 0.028. The SS method had the lowest correlation of egg count at 0.7-2.5 in low cluttered images with $R^2 = 0.788$, MAE = 0.192, and MAPE = 0.074. The CA method had the optimal range of ratio at 0.7-3.5 in low cluttered images with $R^2 = 0.883$, MAE=0.103, and MAPE = 0.037. The EP and CA methods were found to be better in the detection and quantification of RKN as compared to the detection using the PCR (Polymerase Chain Reaction) method. The quantification of root-knot nematodes, lesion nematodes, and dagger nematodes found a correlation of the manual and PCR methods to be R^2=0.83 [17].

The optimal ranges of ratio were different for CA, SS, and EP methods. The main cause of this difference is the length. The perimeter of contour is larger than the distance between two endpoints of RKN eggs. The optimal range of the ratios was also slightly different in the low and high cluttered images for each method due to numerous RKN eggs and soil particles in high cluttered images compared to low

TABLE 6. Comparison of automated and manual root-knot nematode (rkn) eggs count with ratio variation (low-cluttered).

Ratio Range based on average-width	Method	Coefficient of Determination (R^2)	Mean Absolute Error (MAE)	Mean Absolute Percentage Error (MAPE)	Misidentified Root-knot nematode eggs	Detected Root-knot nematode eggs	Undetected Root-knot nematode eggs
	Contour Arc	0.465	0.660	0.254	10	1434	474
0.3-3.5	Skeleton Structure	0.766	0.210	0.084	110	1864	44
	Extreme Point	0.587	0.444	0.174	12	1594	314
	Contour Arc	0.465	0.660	0.254	10	1434	474
0.5-3.5	Skeleton Structure	**0.769**	**0.206**	**0.082**	**107**	**1864**	**44**
	Extreme Point	0.587	0.444	0.174	12	1594	314
	Contour Arc	0.465	0.660	0.254	10	1434	474
0.7-3.5	Skeleton Structure	0.767	0.206	0.082	105	1862	46
	Extreme Point	0.587	0.444	0.174	12	1594	314
	Contour Arc	0.465	0.660	0.254	10	1434	474
1-3.5	Skeleton Structure	0.753	0.210	0.082	98	1852	56
	Extreme Point	0.587	0.444	0.176	12	1591	317
	Contour Arc	0.465	0.660	0.254	10	1434	474
1.3-3.5	Skeleton Structure	0.602	0.341	0.134	78	1736	172
	Extreme Point	0.587	0.444	0.192	11	1562	346
	Contour Arc	0.643	0.349	0.132	22	1674	234
1.3-4	Skeleton Structure	0.602	0.354	0.138	105	1753	155
	Extreme Point	0.713	0.285	0.113	16	1715	193
	Contour Arc	0.760	0.219	0.084	27	1774	134
1.3-4.5	Skeleton Structure	0.602	0.372	0.144	132	1767	141
	Extreme Point	0.771	0.215	0.084	20	1770	138
	Contour Arc	0.791	0.181	0.067	34	1809	99
1.3-5	Skeleton Structure	0.591	0.403	0.157	162	1774	134
	Extreme Point	0.793	0.189	0.074	29	1798	110
	Contour Arc	0.825	0.150	0.055	41	1839	69
1.3-5.5	Skeleton Structure	0.572	0.440	0.171	192	1777	131
	Extreme Point	**0.800**	**0.182**	**0.071**	**37**	**1811**	**97**
	Contour Arc	0.835	0.143	0.053	49	1852	56
1.3-6	Skeleton Structure	0.553	0.466	0.180	214	1780	128
	Extreme Point	0.789	0.195	0.075	52	1817	91
	Contour Arc	0.849	0.132	0.049	55	1866	42
1.3-6.5	Skeleton Structure	0.523	0.496	0.190	237	1781	127
	Extreme Point	0.780	0.210	0.079	68	1820	88
	Contour Arc	**0.851**	**0.132**	**0.048**	**63**	**1874**	**34**
1.3-7	Skeleton Structure	0.510	0.517	0.200	256	1785	123
	Extreme Point	0.746	0.242	0.092	90	1820	88
	Contour Arc	0.850	0.135	0.048	71	1880	28
1.3-7.5	Skeleton Structure	0.499	0.534	0.206	270	1786	122
	Extreme Point	0.727	0.261	0.100	105	1821	87
	Contour Arc	0.848	0.133	0.049	63	1873	35
1.3-8	Skeleton Structure	0.494	0.551	0.212	284	1788	120
	Extreme Point	0.718	0.281	0.107	120	1822	86

TABLE 7. Comparison of automated and manual root-knot nematode (rkn) eggs count with ratio variation (high-cluttered).

Ratio Range based on average-width	Method	Coefficient of Determination (R^2)	Mean Absolute Error (MAE)	Mean Absolute Percentage Error (MAPE)	Misidentified Root-knot nematode eggs	Detected Root-knot nematode eggs	Undetected Root-knot nematode eggs
	Contour Arc	0.597	1.551	0.203	3	1214	312
0.3-3.5	Skeleton Structure	0.805	0.591	0.083	93	1499	27
	Extreme Point	0.630	1.128	0.150	7	1304	222
	Contour Arc	0.597	1.551	0.203	3	1214	312
0.5-3.5	Skeleton Structure	**0.806**	**0.586**	**0.082**	**92**	**1499**	**27**
	Extreme Point	0.630	1.128	0.150	7	1304	222
	Contour Arc	0.597	1.551	0.203	3	1214	312
0.7-3.5	Skeleton Structure	0.803	0.596	0.084	92	1497	29
	Extreme Point	0.630	1.128	0.150	7	1304	222
	Contour Arc	0.597	1.551	0.203	3	1214	312
1-3.5	Skeleton Structure	0.737	0.719	0.101	71	1451	75
	Extreme Point	0.614	1.221	0.161	7	1285	241
	Contour Arc	0.597	1.551	0.203	3	1214	312
1.3-3.5	Skeleton Structure	0.364	2.009	0.262	18	1136	390
	Extreme Point	0.562	1.586	0.210	5	1209	317
	Contour Arc	0.746	0.896	0.116	6	1350	176
1.3-4	Skeleton Structure	0.366	1.857	0.243	30	1179	347
	Extreme Point	0.636	1.285	0.170	11	1276	250
	Contour Arc	0.806	0.635	0.081	11	1408	118
1.3-4.5	Skeleton Structure	0.357	1.812	0.238	35	1193	333
	Extreme Point	0.645	1.201	0.160	20	1302	224
	Contour Arc	0.835	0.517	0.066	16	1437	89
1.3-5	Skeleton Structure	0.358	1.763	0.233	44	1212	314
	Extreme Point	**0.662**	**1.128**	**0.151**	**24**	**1321**	**205**
	Contour Arc	0.827	0.487	0.064	31	1458	68
1.3-5.5	Skeleton Structure	0.362	2.174	0.228	50	1226	300
	Extreme Point	0.652	1.088	0.146	31	1336	190
	Contour Arc	0.826	0.492	0.065	41	1467	59
1.3-6	Skeleton Structure	0.379	1.679	0.223	55	1240	286
	Extreme Point	0.658	1.073	0.144	33	1341	185
	Contour Arc	0.838	0.487	0.066	51	1478	48
1.3-6.5	Skeleton Structure	0.384	1.655	0.220	57	1247	279
	Extreme Point	0.661	1.049	0.141	34	1347	179
	Contour Arc	**0.841**	**0.497**	**0.067**	**61**	**1486**	**40**
1.3-7	Skeleton Structure	0.381	1.630	0.217	61	1256	270
	Extreme Point	0.648	1.034	0.139	39	1355	171
	Contour Arc	0.832	0.527	0.072	68	1487	39
1.3-7.5	Skeleton Structure	0.379	1.625	0.217	63	1259	267
	Extreme Point	0.653	1.019	0.137	45	1364	162
	Contour Arc	0.810	0.576	0.078	80	1489	37
1.3-8	Skeleton Structure	0.385	1.605	0.214	63	1263	263
	Extreme Point	0.658	0.990	0.133	49	1374	152

cluttered images. The optimal ratios range of EP and SS were slightly different for both highly cluttered and lowly cluttered images. This is because highly cluttered images consist of numerous RKN eggs with varied shapes and soil particles.

The number of misidentifications of RKN eggs and undetected eggs were greater in the highly cluttered images because the structure of the soil particles was similar to that of the RKN egg. Some RKN eggs were not detected because their structure was deformed by soil particles attached to them. The soil particles were misidentified as RKN eggs, and the number of undetected eggs were less in the low-cluttered images. The increment in the density of RKN eggs also increased the overlapped eggs and soil particles which could decrease the performance of the RKN egg detection method. Besides these, some soil particles were from the background of the image. The threshold segmentation technique could not discriminate these soil particles. The color segmentation technique was also tested for the sample images. However, RKN eggs have a transparent area between embryo and eggshell that captures the colour of the background. Thus, it hindered the perfect segmentation of RKN eggs.

In addition, the average width of the object was investigated to detect and count the RKN eggs. The CA, SS, and EP methods could not perform well based on average width compared with the mid-width. Nevertheless, the CA method was found to be more accurate than AP and SS. The average width methods showed lower R^2 erroneous outcomes in both lowly-cluttered and highly cluttered images (Table 6 and 7).

The SS method was best suited for the detection of RKN juveniles in a previous study [40]. However, it could not detect RKN eggs with a high level of accuracy. RKN eggs have a transparent feature, making it difficult to obtain a perfect shape during segmentation. In contrast, the image acquisition of live RKN juveniles was hindered by the dorso-ventral waves that originate from head to tail [56]. These waves are formed by the contraction and relaxation of longitudinal muscles on the dorsal and ventral parts of the nematode. The movement of the nematode resulted in the transparent appearance of head and tail parts. Thus, the important features of a juvenile at the head and tail parts were missed in the image. Another problem with live RKN juveniles is the high chance of tangling with each other as their density increases. The RKN egg detection method was not affected by the movement of juveniles [40]. Besides this, the intraspecific variability of morphological features of RKN can hinder the RKN juvenile quantification process [24].

The detection of RKN juvenile relies on the computation of the ratio of body length to greatest body diameter (De Man Formulae). The maximum juvenile body width is found in the middle part of the juvenile body [57]. Hence, the width of the juvenile is calculated in the middle of the juvenile body. As juveniles have irregular structures and shapes, we computed the path of each pair of endpoints in the graph using network/graph theory. The midpoint is computed in the longest path in the graph. But the midpoint of the RKN egg is computed using the centroid of the blob also known as the image moment. Image moment is the weighted average of pixel intensities. The ratio is formulated from the ellipse equation as described in Figure 5 and Table 1.

The skeleton graph method chooses the longest path among multiple paths in the graph to determine the length of the juvenile. The juvenile structure can have many branches due to the deformation of shape, whereas the skeleton structure method used the sum of the two largest branches to calculate the length of the skeleton structure consisting of multiple branches. The CA method used to compute the length of RKN juveniles, and eggs is similar, however the central idea of this algorithm is the use of the ratio of the body length to greatest body diameter. The calculation of the ratio is completely different in the detection of RKN eggs and juveniles. Thus, the algorithm is a modified version of a previously developed algorithm [40]. The skeleton graph method showed better results to detect RKN juveniles, whereas the EP method performed well to detect RKN eggs.

The skeleton structure method significantly reduced the original length of RKN eggs, so it could not achieve optimum detection.

Although the presented method detected the RKN eggs at the optimum level (R^2=0.905), the accuracy of the detection technique could be further improved by using other segmentation techniques such as contrast enhancement to obtain quality images. The RKN egg extraction methods could limit the acquisition of quality images, for examples, maceration of roots from field grown plants could introduce plant tissue; hence optimised methods for RKN egg extraction including sugar centrifugation could be explored to remove soil and particles of plant roots to produce a cleaner extraction. The detection methods used the image segmentation technique, so the increase in the density of objects formed object overlap in the image. Thus, the detection methods could not detect RKN eggs due to their deformed shape. The major challenge to discerning objects in the microscopic image is illumination techniques, transparency of an object, object movement and contrast enhancement constraint.

V. CONCLUSION

This study provided a semi-automated approach to detect and count RKN eggs that could be used instead of manually counting that is associated with fatigue. This method used image processing and computer vision that helps to quantify RKN population and assess the nematode infestation in the host plants. A new EP method was used to measure, detect, and count the RKN eggs and compared with the other two methods. The EP method based on mid-width outperformed EP and SS methods with the correlation of R^2=0.905 to detect and enumerate the RKN eggs in both low and high cluttered images. This investigation supports image analysis techniques to analyse the object shape and develop methods for image annotation. The measurement data analysis showed that the difference between the mid-width and average width could be used to distinguish objects. Also, the width difference was low for bean-shaped eggs compared to the

perfect elliptical structure. This feature can be used to discriminate objects in other object detection and image analysis problems.

VI. FUTURE WORK

The methods developed in this study can be investigated to detect other genus and species of nematode eggs such as the cyst nematodes, or spores of arbuscular mycorrhiza fungi. The RKN egg detection could be investigated with various image acquisition settings with the different objective lens. The segmentation methods such as clustering-based, edge-based, region-based, and neural network segmentation could be explored to discriminate RKN eggs and background soil particles. These object detection methods can analyse the shape and size of objects and automate image labelling tasks essential for machine learning methods. The detection and quantification of RKN eggs can be further extended to machine learning approaches.

A. ABBREVIATIONS AND ACRONYMS

CA: Contour arc
EP: End point
MAE: Mean absolute error
MAPE: Mean absolute percentage error
PCR: Polymerase chain reaction
RKN: Root-knot nematode
R^2: Coefficient of determination
SS: Skeleton structure

ACKNOWLEDGMENT

The authors would like to acknowledge the Research Training Program Scholarship Funded by the Australian Government and all the support provided by Central Queensland University, Australia. They wish special thanks to worldwide researchers for providing valuable information on root-knot nematodes. They would like to thank Dr. Jady Li for her advice during the earlier part of the research and for supplying the RKN Eggs used to inoculate the tomato plants.

REFERENCES

[1] T. Bongers and H. Ferris, "Nematode community structure as a bioindicator in environmental monitoring," *Trends Ecol. Evol.*, vol. 14, no. 6, pp. 224–228, Jun. 1999.
[2] M. Schratzberger, M. Holterman, D. van Oevelen, and J. Helder, "A Worm's world: Ecological flexibility pays off for free-living nematodes in sediments and soils," *BioScience*, vol. 69, no. 11, pp. 867–876, Nov. 2019.
[3] M. M. Shah and M. Mahamood, "Nematology: Concepts, diagnosis and control," in *BoD-Books on Demand*. Rijeka, Croatia: InTechOpen, 2017.
[4] G. C. Bernard, M. Egnin, and C. Bonsi, "The impact of plant-parasitic nematodes on agriculture and methods of control," in *Nematology-Concepts, Diagnosis and Control*, vol. 10. Rijeka, Croatia: InTechOpen, 2017.
[5] A. F. Bird, "The attractiveness of roots to the plant parasitic nematodes meloidogyne javanica and M. Hapla," *Nematologica*, vol. 4, no. 4, pp. 322–335, 1959.
[6] D. B. Dusenbery, "Theoretical range over which bacteria and nematodes locate plant roots using carbon dioxide," *J. Chem. Ecol.*, vol. 13, no. 7, pp. 1617–1624, Jul. 1987.
[7] J.-C. Prot, "Migration of plant-parasitic nematodes towards plant roots," *Revue de Nématologie*, vol. 3, no. 2, pp. 305–318, 1980.
[8] V. M. Williamson and R. S. Hussey, "Nematode pathogenesis and resistance in plants," *Plant Cell*, vol. 8, no. 10, p. 1735, Oct. 1996.
[9] J. T. Jones, "Top 10 plant-parasitic nematodes in molecular plant pathology," *Mol. Plant Pathol.*, vol. 14, no. 9, pp. 946–961, 2013.
[10] J. Nicol, S. Turner, D. Coyne, L. den Nijs, S. Hockland, and Z. T. Maafi, "Current nematode threats to world agriculture," in *Genomics and Molecular Genetics of Plant-Nematode Interactions*. Heidelberg, Germany: Springer, 2011, pp. 21–43.
[11] A. A. Elling, "Major emerging problems with minor meloidogyne species," *Phytopathology*, vol. 103, no. 11, pp. 1092–1102, Nov. 2013.
[12] B. Blair and G. Stirling, "The role of plant-parasitic nematodes in reducing yield of sugarcane in fine-textured soils in Queensland, Australia," *Austral. J. Exp. Agricult.*, vol. 47, no. 5, pp. 620–634, 2007.
[13] S. A. Bhuiyan, B. J. Croft, G. R. Stirling, E. Wong, P. Jackson, and M. Cox, "Assessment of resistance to root-lesion and root-knot nematodes in Australian hybrid clones of sugarcane and its wild relatives," *Australas. Plant Pathol.*, vol. 45, no. 2, pp. 165–173, Apr. 2016.
[14] D. M. Bird and I. Kaloshian, "Are roots special? Nematodes have their say," *Physiol. Mol. Plant Pathol.*, vol. 62, no. 2, pp. 115–123, Feb. 2003.
[15] G. M. Murray and J. P. Brennan, "Estimating disease losses to the Australian wheat industry," *Australas. Plant Pathol.*, vol. 38, no. 6, pp. 558–570, 2009.
[16] S. D. Berry, M. Fargette, V. W. Spaull, S. Morand, and P. Cadet, "Detection and quantification of root-knot nematode (Meloidogyne javanica), lesion nematode (Pratylenchus zeae) and dagger nematode (Xiphinema elongatum) parasites of sugarcane using real-time PCR," *Mol. Cellular Probes*, vol. 22, no. 3, pp. 168–176, Jun. 2008.
[17] G. Uysal, M. A. Sögüt, and İ. H. Elekçioğlu, "Identification and distribution of root-knot nematode species (Meloidogyne spp.) in vegetable growing areas of lakes region in Turkey," *Turkish J. Entomol.*, vol. 41, no. 1, pp. 105–122, Mar. 2017.
[18] M. Burkett-Cadena, N. Kokalis-Burelle, K. S. Lawrence, E. van Santen, and J. W. Kloepper, "Suppressiveness of root-knot nematodes mediated by rhizobacteria," *Biol. Control*, vol. 47, no. 1, pp. 55–59, Oct. 2008.
[19] C. Wang, M. Ulloa, T. R. Mullens, J. Z. Yu, and P. A. Roberts, "QTL analysis for transgressive resistance to root-knot nematode in interspecific cotton (Gossypium spp.) progeny derived from susceptible parents," *PLoS ONE*, vol. 7, no. 4, Apr. 2012, Art. no. e34874.
[20] S. T. Nyaku, H. Lutuf, and E. Cornelius, "Morphometric characterisation of root-knot nematode populations from three regions in Ghana," *Plant Pathol. J.*, vol. 34, no. 6, p. 544, 2018.
[21] K. Huang, Q. Jiang, L. Liu, S. Zhang, C. Liu, H. Chen, W. Ding, and Y. Zhang, "Exploring the key microbial changes in the rhizosphere that affect the occurrence of tobacco root-knot nematodes," *AMB Exp.*, vol. 10, no. 1, pp. 1–11, Dec. 2020.
[22] S. Brown, G. Yeckel, R. Heinz, K. Clark, D. Sleper, and M. G. Mitchum, "A high-throughput automated technique for counting females of Heterodera glycines using a fluorescence-based imaging system," *J. Nematol.*, vol. 42, no. 3, p. 201, 2010.
[23] O. Grillo, M. F. Andrés, and S. Moreno-Vázquez, "Quantitative evaluation of heterodera avenae females in soil and root extracts by digital image analysis," *Crop Protection*, vol. 81, pp. 85–91, Mar. 2016, doi: 10.1016/j.cropro.2015.12.010.
[24] C. Maleita, I. Esteves, J. Cardoso, M. Cunha, R. Carneiro, and I. Abrantes, "Meloidogyne luci, a new root-knot nematode parasitizing potato in Portugal," *Plant Pathol.*, vol. 67, no. 2, pp. 366–376, 2018.
[25] Z. Devran and M. A. Sögüt, "Occurrence of virulent root-knot nematode populations on tomatoes bearing the mi gene in protected vegetable-growing areas of Turkey," *Phytoparasitica*, vol. 38, no. 3, pp. 245–251, Jul. 2010.
[26] A. Vezina. *Root-Knot Nematodes*. ProMusa. Accessed: Sep. 7, 2021. [Online]. Available: https://www.promusa.org/Root-knot+nematodes
[27] D. Orion and G. Kritzman, "A role of the gelatinous matrix in the resistance of root-knot nematode (Meloidogyne spp.) eggs to microorganisms," *J. Nematol.*, vol. 33, no. 4, p. 203, 2001.
[28] A. A. Evans and R. N. Perry, "Survival mechanisms," in *Root-Knot Nematodes*, M. Moens, R. N. Perry, J. L. Starr Eds. Wallingford, U.K.: CABI, 2009, pp. 201–222.
[29] J. D. Eisenback and D. J. Hunt, "General morphology," in *Root-Knot Nematodes*. Oxfordshire, U.K.: CABI, 2009, pp. 18–54.
[30] S. Thapa, J. A. Patel, U. Reuter-Carlson, and N. E. Schroeder, "Embryogenesis in the parasitic nematode heterodera glycines is independent of host-derived hatching stimulation," *BMC Develop. Biol.*, vol. 17, no. 1, Jan. 2017, doi: 10.1186/s12861-016-0144-7.

[31] T. Mukhtar, M. A. Hussain, M. Z. Kayani, and M. N. Aslam, "Evaluation of resistance to root-knot nematode (Meloidogyne incognita) in okra cultivars," *Crop Protection*, vol. 56, pp. 25–30, Feb. 2014.
[32] S. Nagachandrabose, "Liquid bioformulations for the management of root-knot nematode, meloidogyne hapla that infects carrot," *Crop Protection*, vol. 114, pp. 155–161, Dec. 2018.
[33] S. A. Bhuiyan, K. Garlick, J. M. Anderson, P. Wickramasinghe, and G. R. Stirling, "Biological control of root-knot nematode on sugarcane in soil naturally or artificially infested with pasteuria penetrans," *Australas. Plant Pathol.*, vol. 47, no. 1, pp. 45–52, Jan. 2018.
[34] A. Amadesi, A. Bosco, L. Rinaldi, G. Cringoli, E. Claerebout, and M. P. Maurelli, "Cattle gastrointestinal nematode egg-spiked faecal samples: High recovery rates using the mini-FLOTAC technique," *Parasites Vectors*, vol. 13, no. 1, pp. 1–7, Dec. 2020.
[35] J. L. Roberts and R. A. Swan, "Quantitative studies of ovine haemonchosis. I. Relationship between faecal egg counts and total worm counts," *Veterinary Parasitol.*, vol. 8, no. 2, pp. 165–171, May 1981.
[36] L. E. Ostergaard, "Automatic Detection and characterization of parasite egg by image processing," M.S. thesis, Dept. Mech. Eng., Virginia Polytech. Inst. State Univ., Blacksburg, VA, USA, 2013.
[37] F. Qazi, A. Khalid, A. Poddar, J.-P. Tetienne, A. Nadarajah, A. Aburto-Medina, E. Shahsavari, R. Shukla, S. Prawer, A. S. Ball, and S. Tomljenovic-Hanic, "Real-time detection and identification of nematode eggs genus and species through optical imaging," *Sci. Rep.*, vol. 10, no. 1, pp. 1–12, Dec. 2020.
[38] N. Vovlas, D. Mifsud, B. B. Landa, and P. Castillo, "Pathogenicity of the root-knot nematode Meloidogyne javanica on potato," *Plant Pathol.*, vol. 54, no. 5, pp. 657–664, 2005.
[39] X. Ji, J. Li, B. Dong, H. Zhang, S. Zhang, and K. Qiao, "Evaluation of fluopyram for southern root-knot nematode management in tomato production in China," *Crop Protection*, vol. 122, pp. 84–89, Aug. 2019.
[40] T. B. Pun, A. Neupane, and R. Koech, "Quantification of root-knot nematode infestation in tomato using digital image analysis," *Agronomy*, vol. 11, no. 12, p. 2372, Nov. 2021.
[41] R. Hussey and K. Barker, "A comparison of methods of collecting inocula of Meloidogyne spp., including a new technique," *Plant Dis. Rep.*, vol. 57, pp. 1025–1028, Feb. 1973.
[42] G. W. Zack, W. E. Rogers, and S. A. Latt, "Automatic measurement of sister chromatid exchange frequency," *J. Histochem. Cytochem.*, vol. 25, no. 7, pp. 741–753, 1977.
[43] R. Tajima and Y. Kato, "Comparison of threshold algorithms for automatic image processing of Rice roots using freeware ImageJ," *Field Crops Res.*, vol. 121, no. 3, pp. 460–463, Apr. 2011, doi: 10.1016/j.fcr.2011.01.015.
[44] N. Jamil, T. M. T. Sembok, and Z. A. Bakar, "Noise removal and enhancement of binary images using morphological operations," in *Proc. Int. Symp. Inf. Technol.*, vol. 4, 2008, pp. 1–6.
[45] R. M. Haralick, S. R. Sternberg, and X. Zhuang, "Image analysis using mathematical morphology," *IEEE Trans. Pattern Anal. Mach. Intell.*, vol. PAMI-9, no. 4, pp. 532–550, Jul. 1987.
[46] J. Harrison and A. Norton, "The gauss-green theorem for fractal boundaries," *Duke Math. J.*, vol. 67, no. 3, pp. 575–588, Sep. 1992.
[47] J. Nunez-Iglesias, A. J. Blanch, O. Looker, M. W. Dixon, and L. Tilley, "A new Python library to analyse skeleton images confirms malaria parasite remodelling of the red blood cell membrane skeleton," *PeerJ*, vol. 6, p. e4312, Feb. 2018.
[48] H. I. Choi, S. W. Choi, and H. P. Moon, "Mathematical theory of medial axis transform," *Pacific J. Math.*, vol. 181, no. 1, pp. 57–88, 1997.
[49] S. Nakagawa, P. C. D. Johnson, and H. Schielzeth, "The coefficient of determination R 2 and intra-class correlation coefficient from generalized linear mixed-effects models revisited and expanded," *J. Roy. Soc. Interface*, vol. 14, no. 134, Sep. 2017, Art. no. 20170213.
[50] O. Renaud and M.-P. Victoria-Feser, "A robust coefficient of determination for regression," *J. Statist. Planning Inference*, vol. 140, pp. 1852–1862, Sep. 2010.
[51] S. Dhar Choudhury and S. Pandey, "Nth absolute root mean error," 2018, *arXiv:1810.00421*.
[52] C. J. Willmott and K. Matsuura, "Advantages of the mean absolute error (MAE) over the root mean square error (RMSE) in assessing average model performance," *Climate Res.*, vol. 30, no. 1, pp. 79–82, 2005.
[53] S. E. Razavi, A. Arefi, G. Ledwich, G. Nourbakhsh, D. B. Smith, and M. Minakshi, "From load to net energy forecasting: Short-term residential forecasting for the blend of load and PV behind the meter," *IEEE Access*, vol. 8, pp. 224343–224353, 2020.
[54] L. C. M. de Paula, A. S. Soares, T. W. de Lima, A. C. B. Delbem, C. J. Coelho, and A. R. G. Filho, "A GPU-based implementation of the firefly algorithm for variable selection in multivariate calibration problems," *PLoS ONE*, vol. 9, no. 12, Dec. 2014, Art. no. e114145.
[55] D. Chicco, M. J. Warrens, and G. Jurman, "The coefficient of determination R-squared is more informative than SMAPE, MAE, MAPE, MSE and RMSE in regression analysis evaluation," *PeerJ Comput. Sci.*, vol. 7, p. e623, Jul. 2021.
[56] H. R. Wallace, "The dynamics of nematode movement," *Annu. Rev. Phytopathol.*, vol. 6, no. 1, pp. 91–114, Sep. 1968.
[57] M. Mazurkiewicz, B. Górska, E. Jankowska, and M. Włodarska-Kowalczuk, "Assessment of nematode biomass in marine sediments: A semi-automated image analysis method," *Limnol. Oceanogr., Methods*, vol. 14, no. 12, pp. 816–827, 2016.

TOP BAHADUR PUN received the Bachelor of Computer Engineering degree from Pokhara University and the M.Sc. degree in computer science from Tribhuwan University, Nepal. He is currently pursuing the Doctor of Philosophy degree with CQUniversity. His research interests include computer vision, data analytics, deep learning, and machine learning.

ARJUN NEUPANE received the Bachelor of Computer Application degree from Pokhara University, MIT, Nepal, the Ph.D. degree in information systems from the University of Southern Queensland (UniSQ), Australia, the Graduate Certificate in higher education from Griffith University, and the Graduate Certificate in data science from the University of Queensland, Australia. He is currently a Lecturer with ICT, CQUniversity, Rockhampton, Australia. His main research interests include information systems, data science, machine learning, deep learning, AI, and image processing. He is interested in applying IT to solve real-world problems in different domains. He is a member and a Certified Professional of the Australian Computer Society.

RICHARD KOECH received the B.Sc. degree in agricultural engineering from Egerton University, Kenya, the Master of Engineering Technology degree, and the Ph.D. degree from the University of Southern Queensland, Australia. He is currently a Senior Lecturer with the College of Science and Sustainability, CQUniversity, Australia. His current research interests include soil and agricultural water management, agricultural irrigation, and remote sensing and spatial analysis.

KIRSTY J. OWEN received the B.Sc. (agriculture), M.Sc., and Ph.D. degrees from The University of Sydney, Australia. She is currently a Research Fellow and a Lecturer with the University of Southern Queensland, Australia, and an internationally recognized expert in the management of root-lesion nematodes in grain crops. Her research interests include biotic constraints to crop production within farming systems, particularly interactions between nematodes, soilborne diseases, and beneficial arbuscular mycorrhizal fungi. Her teaching in plant science and agriculture draws on her experiences in applied research and communication of research outcomes with the rural community.